# Effects of 'Sharpness' of the Plasma Cross-Section on the Stability of Peeling-Ballooning Modes in Tokamaks

N. Aiba, S. Tokuda, T. Takizuka, G. Kurita, and T. Ozeki

Japan Atomic Energy Agency, Naka, Ibaraki-ken, 311-0193 Japan

e-mail: aiba.nobuyuki@jaea.go.jp

**Abstract.** Stabilities of a peeling, a ballooning and a peeling-ballooning modes, which relate to edge-localized modes (ELMs), are investigated numerically with the linear ideal magnetohydrodynamic (MHD) stability code MARG2D. Effects of 'sharpness' on the stability of the peeling-ballooning mode are examined, where the sharpness is defined in terms of the curvature at the top and bottom of the outermost flux surface. It is found that the stability limit of the pressure gradient significantly improves as the sharpness increases even when the ellipticity and the triangularity are unchanged. The sharpness is an important parameter for high performance H-mode operations with high pedestal pressure.

## 1 Introduction

An ideal magnetohydrodynamic (MHD) instability in the tokamak edge region is one of the causes of edge-localized modes (ELMs), which constrain the maximum pressure gradient in the edge pedestal of H-mode plasmas[1]. Theoretical researches about ELMs triggered by ideal MHD modes (a peeling mode, a ballooning mode and a peeling-ballooning mode at intermediate $n$) have been developed recently, where $n$ is the toroidal mode number. For example, the linear stability analyses showed that the stability of the peeling-ballooning modes depends on the shape of the equilibrium (the ellipticity $\delta$, the triangularity $\kappa$[2], the squareness $Sq$[3] and so on). These results are consistent with the change of the ELMs phenomena observed experimentally[4, 5]. Recently, the shape of the top of the equilibrium is shown experimentally as the important factor for the ELMy H-mode confinement property[6, 7]. In this paper, we analyze numerically the effect of the 'sharpness' on the stability of the peeling-ballooning modes with the linear ideal MHD stability code MARG2D[8, 9, 10], where the sharpness is defined in terms of the curvature at the top and bottom of the equilibrium. This code solves the eigenvalue problem for the two-dimensional Newcomb equation[11], and gives accurately an equilibrium marginal stability against ideal MHD modes[8, 9]. Due in part to the vacuum energy integral calculation by using a vector potential method, a stability analysis of ideal MHD modes from low to high $n$ is realized on the basis of the single physical model[10].

## 2 Equilibrium properties

### 2.1 Definition of the 'sharpness'

In this section, we first introduce the new shaping parameter 'sharpness' for investigating the effect of the shape of the top or the bottom of the equilibrium on the stability of tokamak edge plasma. This parameter is defined with the curvature at the top or the bottom of the equilibrium as $\sigma = (1/r_c)/(1/a)$, where $r_c$ is the radius of the circle of curvature and $a$ is the plasma minor radius. Figure 1 shows example curvature radii at the top for the pointed (red) and rounded (blue) surfaces. This parameter obviously increases as the plasma shape becomes sharpened. Note that the 'sharpness' does not directly depend on $\kappa$ and $\delta$.

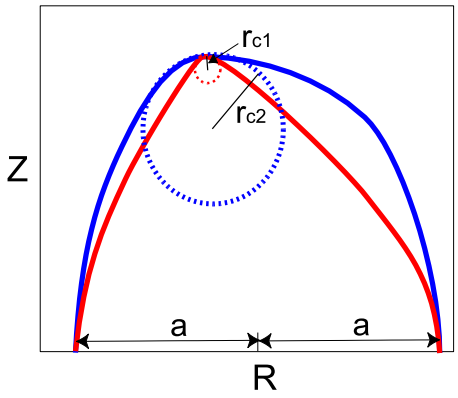


*FIG. 1: Curvature radius at the top of the equilibrium. The sharpness $\sigma$ of the pointed surface (red), $\sigma_1 = (1/r_{c1})/(1/a)$, is larger than that of the rounded one (blue), $\sigma_2 = (1/r_{c2})/(1/a)$.*

### 2.2 Equilibrium properties

For investigating the effect of the sharpness on the stability of a tokamak edge plasma, we analyze the stability of a series of equilibria, whose sharpness of the top of the equilibrium $\sigma_{up}$ are 5.66, 3.19 and 1.75. Hereafter, the equilibria whose $\sigma_{up} = 5.66$, 3.19 and 1.75 are called EQ1, EQ2, and EQ3, respectively. Figure 2(a) shows contours of $\psi$ (magnetic surfaces) of $\sigma_{up}$ =5.66 (EQ1, solid), 3.19 (EQ2, broken), and 1.75 (EQ3, dotted) equilibria. The following parameters of these three equilibria are set as the same; $R_0[m] = 3.19$, $a[m] = 0.88$, $\kappa_{up} = 1.57$, $\kappa_{dw} = 1.75$, $\delta_{up} = 0.20$, $\delta_{dw} = 0.26$, $Sq_{dw}$ and $\sigma_{dw}$, where $R_0$ is the major radius and the subscript $up$ ($dw$) means the up (down) side value. Values of $Sq_{up}$ for EQ2 and EQ3 are the same as each other, but they are larger than that for EQ1.

Profiles of the pressure gradient and the averaged parallel current density are given as

$$\frac{dp}{d\psi} \propto (1-\psi_N^{0.8})^{1.5} + C_p \left( \exp\left( -\frac{(\psi_N - 0.96)^2}{2 \times (0.025)^2} \right) \right), \tag{1}$$

$$\frac{\langle j_{//} \rangle}{\langle B \rangle} = \frac{\langle \boldsymbol{j} \cdot \boldsymbol{B} \rangle}{\langle B^2 \rangle} \propto (1-\psi_N^{0.55})^{2.2} + 0.3 \cdot (1-\psi_N^5) + C_j \left( \exp\left( -\frac{(\psi_N - 0.96)^2}{2 \times (0.025)^2} \right) \right). \tag{2}$$

Here $\psi$ is the poloidal magnetic flux, $\psi_N$ is the poloidal flux normalized as $\psi_N = 0$ at the magnetic axis and $\psi_N = 1$ at the plasma surface, $\boldsymbol{j}$ is the plasma current density, $j_{//}$ is the current density parallel to the magnetic field $\boldsymbol{B}$, and the bracket $\langle X \rangle$ expresses the flux surface average of a variable $X$. The pressure gradient and the current density near $\psi_N = 0.96$ are changed by adjusting the parameters $C_p$ and $C_j$, which are used to express the edge pedestal and the virtual bootstrap current. The poloidal beta value $\beta_p$ is fixed as 0.8 and the toroidal magnetic field at the center of the plasma is 3.5[T] in each equilibrium. Since the plasma currents are given as $I_p[MA] = 1.55$ (EQ1), 1.535 (EQ2), and 1.574 (EQ3), the plasma edge safety factors $q_{edge}$ of these equilibria are similar to each other when the parameter $C_j$ is fixed.

Figure 2(b) shows the profiles of $p$, $dp/d\psi$ and Fig.2(c) shows those of the safety factor $q$ and $\langle j_{//} \rangle / \langle B \rangle$), respectively. In this case, the parameters $C_p$ and $C_j$ are 1.0 and 0.3, and the $q_{edge}$ values are almost same as about 7.52. The positions of maximum pressure gradient and the peak of the pedestal are $\psi_N$ =0.96 and $\psi_N$=0.92, respectively.

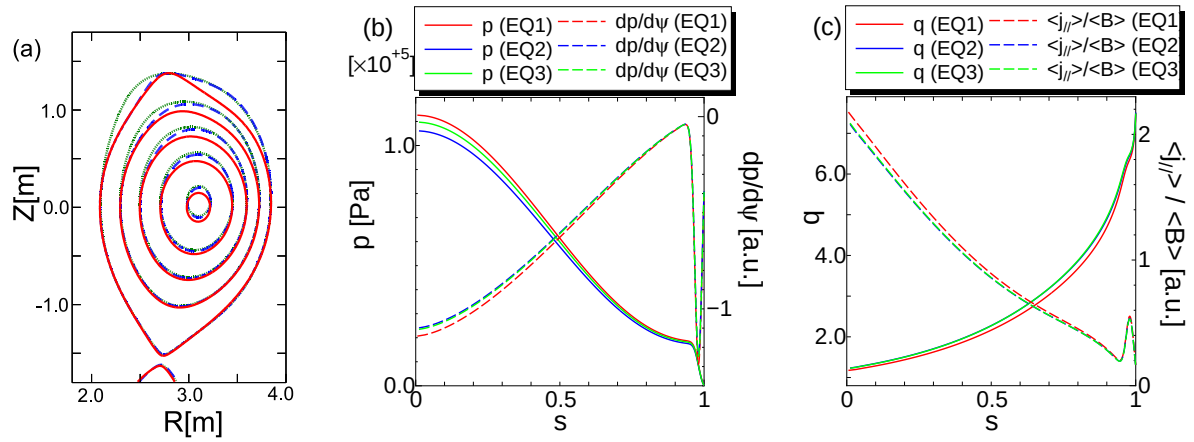


*FIG. 2: (a) Magnetic surfaces for equilibria EQ1 ($\sigma_{up}$ =5.66, red solid line), EQ2 (3.19, blue broken line), and EQ3 (1.75, green dotted line). The ellipticity and triangularity are fixed in each equilibrium. (b) Profiles of the pressure p and the pressure gradient $dp/d\psi$. (c) Profiles of the safety factor q and the parallel current density $j_{//}/\langle B\rangle$. The transverse scale $s = \sqrt{\psi_N}$. The parameters ($C_p$, $C_j$) in Eqs.(1) and (2) are (1.0, 0.3).*

## 3 Effect of the sharpness on the stability of peeling-ballooning modes

The effect of the sharpness on the stability of a tokamak edge plasma is investigated numerically. The stability of the infinite-$n$ ballooning mode is identified by the BETA code[12], and the finite-$n$ ideal MHD mode stability is analyzed with the MARG2D code. The range of $n$ number of the modes to be analyzed is from 1 to 30.

Figure 3(a) shows the stability of the ballooning mode and the peeling-ballooning modes on the $j_{edge}/\langle j_{//}\rangle - \alpha_{96}$ diagram, where $j_{edge}$ is the averaged current density parallel to the magnetic field at the plasma edge, $\alpha$ is the normalized pressure gradient defined as $\alpha = -2\mu_0 R q^2 (dp/dr)/B^2$, $\mu_0$ is the permeability in the vacuum, $r$ is the minor radius of each magnetic surface, and the subscript 96 means the value at $\psi_N = 0.96$. The $n$ number of the most unstable mode near the intersection of the stability boundary of the ballooning mode, calculated with BETA, with that of the peeling-ballooning mode, identified with MARG2D, is about 25 in each equilibrium. Since the $q_{edge}$ value remains fixed for the same value of $(j_{edge}/\langle j_{//}\rangle)$, the maximum $(j_{edge}/\langle j_{//}\rangle)$ value against peeling (kink) modes is almost unchanged as about 0.29, which hardly depends on $\alpha_{96}$. This result shows that the increase of $\sigma_{up}$ has little impact on the stability of current driven (peeling and kink) modes. On the other hand, the maximum $\alpha$ value, which is restricted by the peeling-ballooning mode, improves from 3.22 to 4.38 as $\sigma_{up}$ increases from 1.94 to 5.66. Similarly, from the $s-\alpha$ diagram at $\psi_N = 0.96$ shown in Fig.3(b), we find that the second stable region against the ballooning mode becomes broader as $\sigma_{up}$ increases, where $s$ is the magnetic shear defined as $s = r(dq/dr)/q$. From these results, we reveal that the increase of the sharpness stabilizes the ballooning mode and the peeling-ballooning mode. This improves the stability limit of the pressure gradient at the pedestal of H-mode plasma.

Figure 4 shows the mode structure of the peeling-ballooning mode at the marginally stable condition of (a) EQ1, (b) EQ2, and (c) EQ3 in $(R, Z)$ plane. In this case, the parameters ($j_{edge}/\langle j_{//}\rangle$, $s_{96}$, $\alpha_{96}$) are (0.29, 1.84, 4.38) in EQ1, (0.28, 1.86, 3.65) in EQ2, and (0.27, 1.92, 3.22) in EQ3, respectively. The toroidal mode number $n$ of these modes are identical to each other as $n = 5$. The structures of these modes are similar to each other and localize at the low field side (unfavorable curvature side). This result indicates

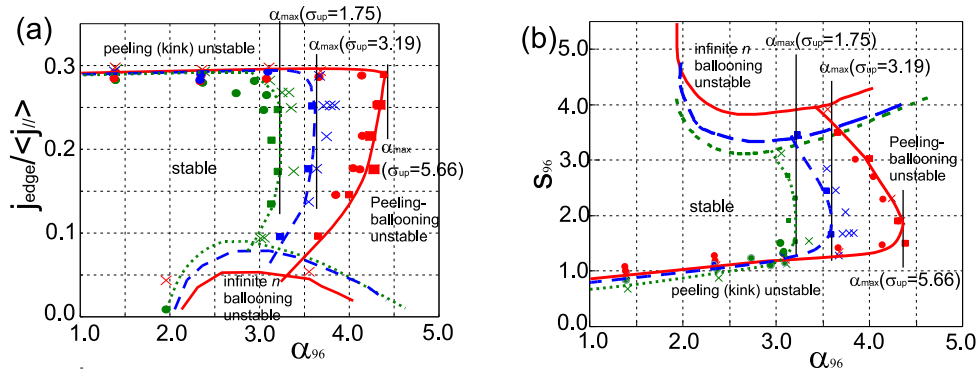


*FIG. 3: (a) Stability of the ballooning mode and that of the peeling-ballooning modes on the $(j_{edge}/\langle j_{//}\rangle - \alpha)$ diagram at $\psi_N = 0.96$ for EQ1 ($\sigma_{up} = 5.66$, red solid line), EQ2 (3.19, blue broken line), and EQ3 (1.94, green dotted line). The limit value of $\alpha$ improves from 3.22 (EQ3) to 3.65 (EQ2) and 4.38 (EQ1) as $\sigma_{up}$ increases. (b) Stability of the ballooning mode ant that of the peeling-ballooning modes on the $s_{96} - \alpha_{96}$ diagram for EQ1, EQ2, and EQ3. The second stability region extends as $\sigma_{up}$ increases.*

that the sharpness stabilizes the ballooning mode and the peeling-ballooning mode, but from the viewpoint of a width of the eigenfunction, this parameter will have little influence on the amount of energy loss by destabilizing the peeling-ballooning mode.

## 4 Mechanism of the stabilization with the sharpness

In this section, we investigate the mechanism of the stabilizing effect of the sharpness. Since we pay attention to the maximum pressure gradient at the pedestal, we confirm the difference between $\sigma_{up} = 5.66$ (EQ1) and 1.75 (EQ3) of the marginally stable condition whose stable pressure gradient limit $\alpha$ is maximum. In this case, the parameter $(j_{edge}/\langle j_{//}\rangle, s_{96}, \alpha_{96})$ are (0.29, 1.84, 4.38) in EQ1 and (0.27, 1.92, 3.22) in EQ3, and the marginally stable eigenfunctions, whose $n$ number is 5, are already shown in Figs.4(a) and (c).

### 4.1 Comparison of the plasma potential energy

On the basis of the ideal MHD model with the incompressible assumption, the plasma potential energy is composed of four terms,

$$\delta W_p = \frac{1}{2}\int \frac{1}{\mu_0}|\boldsymbol{Q}_\perp|^2 + \frac{1}{\mu_0}\left|Q_{//}\boldsymbol{b} - \mu_0\frac{\boldsymbol{\xi}\cdot\nabla p}{B^2}\boldsymbol{B}\right|^2 - \frac{\boldsymbol{j}\cdot\boldsymbol{B}}{B^2}(\boldsymbol{\xi}\times\boldsymbol{B})\cdot\boldsymbol{Q} - 2(\boldsymbol{\xi}\cdot\nabla p)(\boldsymbol{\xi}\cdot\boldsymbol{\kappa})\sqrt{g}d\tau. \quad (3)$$

Here $\boldsymbol{Q} = \boldsymbol{Q}_\perp + Q_{//}\boldsymbol{b} = \nabla\times(\boldsymbol{\xi}\times\boldsymbol{B})$ is the perturbed magnetic field, the subscript $\perp$ expresses the value perpendicular to the equilibrium magnetic field $\boldsymbol{B}$, $\boldsymbol{\xi}$ is the plasma displacement, $\boldsymbol{\kappa}$ is the curvature of $\boldsymbol{B}$, and $\sqrt{g}$ is the Jacobian. The first and second terms of the right hand side of Eq.(3) are the stabilizing terms called the shear Alfvén term and the compressional Alfvén term. On the other hand, the third and forth terms express the destabilizing terms driven by the parallel current and the pressure gradient, respectively. In this subsection, we calculate these components of the potential energy, and compare them in EQ1 and EQ3.

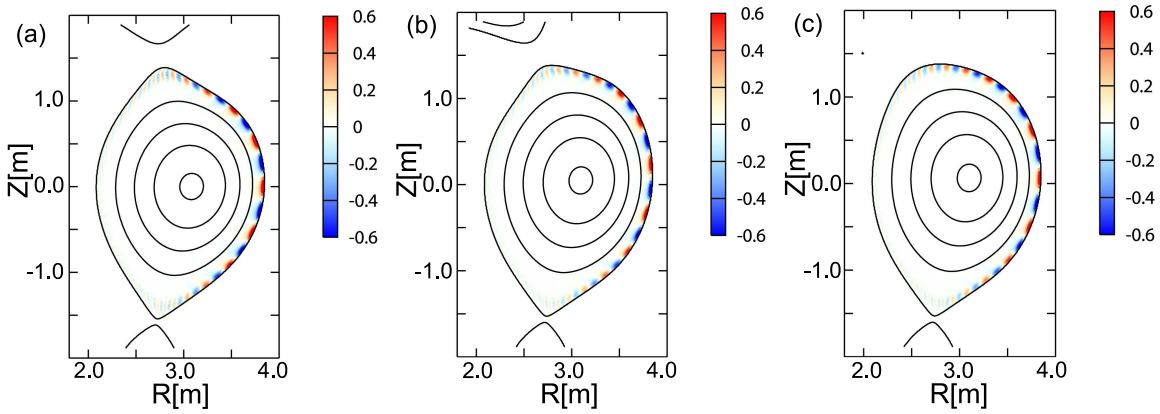


*FIG. 4: Mode structures of the marginally stable peeling-ballooning mode of (a) EQ1, (b) EQ2, and (c) EQ3 in (R, Z) plane. The parameters ($j_{edge}/\langle j_{//}\rangle$, $s_{96}$, $\alpha_{96}$) are (0.29, 1.84, 4.38) in EQ1, (0.28, 1.86, 3.65) in EQ2, and (0.27, 1.92, 3.22) in EQ3, respectively. These modes, whose n numbers are same as 5, localize at the low field side, and the mode structures are similar to each other.*

Figure 5 shows the components of the potential energy of (a) EQ1 and (b) EQ3. In this case, the compressional Alfvén component, shown with the yellow dotted-broken line, hardly contributes to the plasma potential energy, and the stability is determined by the difference between the shear Alfvén term (aqua dotted line) and the sum of the current driven (red solid line) and the pressure driven (blue broken line) terms. The ratio among the integral of the shear Alfvén term, that of the current driven term and that of the pressure driven term is about $7 : -5 : -2$ ($13 : -9 : -4$) in EQ1 (EQ3). This indicates that the dominant destabilizing component is the parallel current, but the contribution from the plasma pressure is not negligible in these marginally stable conditions of EQ1 and EQ3.

Figure 5(c) shows the comparison of the destabilizing terms between EQ1 (solid line) and EQ3 (broken line). Though the profile of the current driven component (red) and that of the pressure driven component (blue) of EQ1 are different from those of EQ3, the sum of these terms, shown with the green lines in Fig.5(c), are almost same as each other.

From this result, we confirm that the increase of the sharpness does not change the threshold of the destabilizing energy, which is driven by the parallel current and the pressure gradient.

### 4.2 Comparison of the eigenfunction in the poloidal direction

In Section 3, we reveal that the sharpness can stabilize the ballooning mode but has little impact on the current driven mode stability. With the objective of the ballooning mode stability, we pay attention to the structure of the eigenfunction in the poloidal direction. In EQ1 and EQ3, the marginally stable $n = 5$ eigenfunction determines the stability limit of the pressure gradient limit. Figure 6 shows the mode structure of the eigenfunction in the poloidal direction, where the transverse scale $\theta$ is the poloidal angle in the straight field line coordinate ($\psi$, $\theta$, $\phi$). As shown in Fig.6(a), the mode structures in EQ1 (red) and EQ3 (blue) at $\psi_N = 0.96$ are similar to each other. However, at $\psi_N = 0.98$ and 0.99 shown in Figs.6 (b) and (c), the eigenfunction in EQ1 is more localized near $\theta = 0$ than that in EQ3. The broadenings of the eigenfunctions in both equilibria are also suppressed near $\theta = -0.4\pi$, where is the bottom of the equilibrium. The reason of the localization is obviously that the trial function which has finite amplitude near the top and the bottom

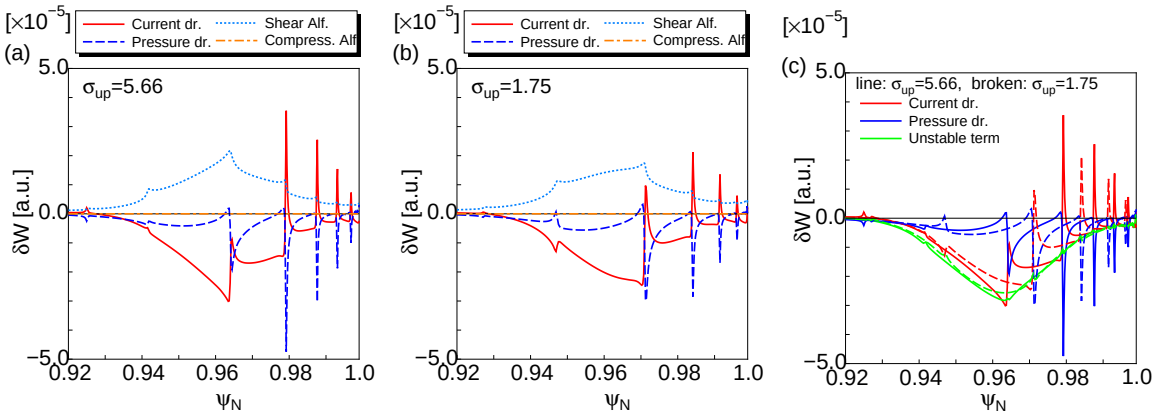


*FIG. 5: Components of the potential energy in Eq.(3) of (a) EQ1 and (b) EQ3. The red solid, blue broken, aqua dotted and yellow doted-broken lines express the current driven, pressure driven, shear Alfvén and compressional Alfvén terms, respectively. (c) Comparison of the current driven terms (red), pressure driven terms (blue), and sum of them (green) between EQ1 (solid line) and EQ3 (broken line).*

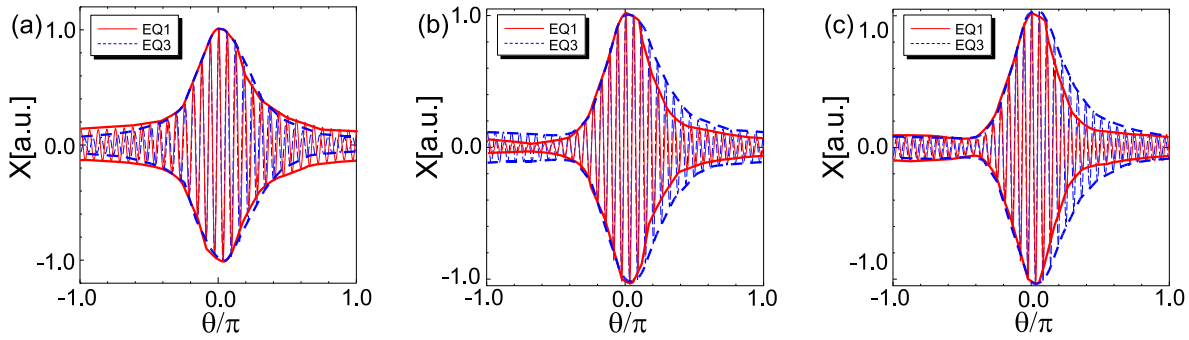


*FIG. 6: Mode structure of the eigenfunction in the poloidal direction at (a) $\psi_N = 0.96$, (b) 0.98 and (c) 0.99. The structure of the eigenfunction in EQ1 (EQ3) is shown with the red solid (blue broken) line.*

of the equilibrium increases the plasma potential energy.

On the basis of the results that the increase of the sharpness localizes the eigenfunction in the poloidal direction and extends the second region of ballooning mode stability as shown in Fig.3(b), the stability boundary of the peeling-ballooning mode, destabilized by both the parallel current and the pressure gradient, is improved by stabilizing mainly the pressure driven component with the increase of the sharpness.

### 4.3 Comparison of the equilibrium quantities affecting the ballooning mode stability

In the previous subsection, we reason that the stabilization of the ballooning mode by increasing the sharpness has an impact on stabilizing the peeling-ballooning mode. From this viewpoint, we compare the equilibrium quantities which affect the ballooning mode stability.

In the limit of large toroidal mode number $n$, the stability of the ideal ballooning mode

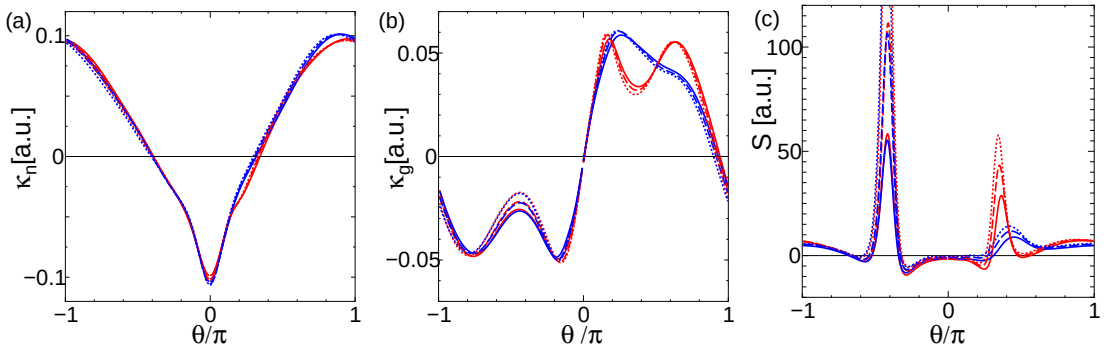


*FIG. 7: Profiles of (a) $\kappa_n$, (b) $\kappa_g$ and (c) s of EQ1 (red) and EQ3 (blue) in the poloidal direction. The solid, broken, and dotted lines express the values at $\psi_N = 0.96$, 0.98 and 0.99, respectively,*

can be determined by the ballooning equation[13, 14, 15]

$$\boldsymbol{B}\cdot\nabla\left[\left(\frac{1}{|\nabla\psi|^2}+\frac{|\nabla\psi|^2}{B^2}I^2\right)(\boldsymbol{B}\cdot\nabla)\boldsymbol{\xi}\right] + \left(\frac{2}{B^2}\frac{dp}{d\psi}\left[\frac{B^2}{|\nabla\psi|^2}\kappa_n + I\kappa_g\right] + \rho\omega^2\left(\frac{1}{|\nabla\psi|^2}+\frac{|\nabla\psi|^2}{B^2}I^2\right)\right)\boldsymbol{\xi} = 0, \tag{4}$$

$$I = \int\frac{S}{B}dl, \tag{5}$$

$$S = -\frac{\nabla\psi\times\boldsymbol{B}}{|\nabla\psi|^2}\cdot\left(\nabla\times\left(\frac{\nabla\psi\times\boldsymbol{B}}{|\nabla\psi|^2}\right)\right), \tag{6}$$

where $S$ is called the local shear, $\kappa_n = \boldsymbol{\kappa}\cdot\nabla\psi$ is the normal curvature and $\kappa_g = \boldsymbol{\kappa}\cdot(\nabla\psi\times\boldsymbol{B})$ is the geodesic curvature. These quantities $\kappa_n$, $\kappa_g$ and $S$ play important roles in ballooning stability theory[15, 16].

Figure 7 shows the $\theta$ dependence of (a) $\kappa_n$, (b) $\kappa_g$ and (c) $S$ at $\psi_N = 0.96$ (solid line), 0.98 (broken line) and 0.99 (dotted line), respectively. From these figures, we find that the profiles of $\kappa_g$ and $S$ of EQ1 (red) near $\theta = 0.4$ are different from those of EQ3 (blue), though there is little appreciate change of $\kappa_n$. In particular, the increase of $S$ impacts the stability of ballooning mode in the second region of stability. Since the large absolute value of $S$ stabilizes a pressure driven mode, the broadening of the most unstable eigenfunction in the poloidal direction will be restricted to the region where $S$ is small and $\kappa_n$ is negative. This is consistent with the result shown in Figs.6(b) and (c).

These results indicate that the shaping parameter sharpness affects the stability of the ballooning mode and the peeling-ballooning mode through changing the local shear near the top or the bottom of the equilibrium.

## 5 Summary

We have introduced the new plasma shaping parameter 'sharpness' to identify the effect of the shape at the top or the bottom of the equilibrium on the stability of tokamak edge plasma. The result of the numerical stability analysis of an infinite-$n$ ballooning mode and finite-$n$ ideal MHD modes have showed that the increase of the sharpness stabilizes the ballooning mode and the peeling-ballooning mode, though a current driven kink (peeling) mode is hardly stabilized. This stabilizing effect of the sharpness has an impact on the stability of the pressure driven ballooning mode mainly through multiplying the local

shear near the top or the bottom of the equilibrium. These results have revealed for the first time that the plasma pressure at the pedestal can be improved by increasing the sharpness; in other words, the sharpness is an important factor for an H-mode operation with a high confinement performance.

### Acknowledgments

The authors would like to thank Dr. M. Kikuchi and Dr. H. Ninomiya for their support.

### References

[1] J. W. Connor, R. J. Hastie, H. R. Wilson, and R. L. Miller, Phys. Plasmas **5**, 2687 (1998).

[2] P. B. Snyder, H. R. Wilson, J. R. Ferron, L. L. Lao, A. W. Leonard, D. Mossessian, M. Murakami, T. H. Osborne, A. D. Turnbull, and X. Q. Xu, Nucl. Fusion **44**, 320 (2004).

[3] A. W. Leonard, T. H. Osborne, P. B. Snyder, R. J. Groebner, P. Gohil, Bull, Am. Phys. Soc. **50**, 270 (2005).

[4] J. R. Ferron et al., Phys. Plasmas, **7**, 1976 (2000).

[5] Y. Kamada, H. Takenaga, A. Isayama, T. Hatae, H. Urano, H. Kubo, T. Takizuka and Y. Miura, Plasma Phys. Control. Fusion **44**, A279 (2002).

[6] S. Takeji et al., Fusion Sci. Technol. **42**, 278 (2002).

[7] T. Takizuka, H. Urano, H. Takenaga and N. Oyama, Phys. Control. Fusion **48**, 799 (2006).

[8] S. Tokuda and T. Watanabe, Phys. Plasmas **6**, 3012 (1999).

[9] S. Tokuda, N. Aiba and M. Okamoto, TH/P4-46, 20th IAEA Fusion Energy Conference, 2004.

[10] N. Aiba, S. Tokuda, T. Ishizawa and M. Okamoto, Comput. Phys. Commun. **175**, 269 (2006).

[11] W. A. Newcomb, Ann. Phys. **232**, 10 (1960).

[12] M. Azumi et al., Plasma Phys. (Proc. 6th Int. Conf., Lausanne, 1984) vol 1 (Brussels: CEC) 375 (1984).

[13] D. Dobrott, D. B. Nelson, J. M. Greene, A. H. Glasser, M. S. Chance, and E. A. Frieman, Phys. Rev. Lett. **39**, 943 (1977).

[14] J. W. Connor, R. J. Hastie, and J. B. Taylor, Phys. Rev. Lett. **40**, 396 (1978).

[15] M. S. Chance, S. C. Jardin, and T. H. Stix, Phys. Rev. Lett. **51**, 1963 (1983).

[16] J. M. Greene, M. S. Chance, Nucl. Fusion **21**, 453 (1981).